Combinatorial sample preparation platform for droplet-based applications in microbiology

Ashkan Samimi [a,b], Sundar Hengoju [a], Miriam A. Rosenbaum [a,b,c,*]

[a] *Leibniz Institute for Natural Product Research and Infection Biology - Hans Knöll Institute, Jena, Germany*
[b] *Faculty of Biological Sciences, Friedrich Schiller University, Jena, Germany*
[c] *Cluster of Excellence Balance of the Microverse, Friedrich Schiller University Jena, Jena, Germany*

ABSTRACT

Droplet microfluidics has demonstrated immense potential in microbiological studies due to its unique features, such as miniaturization, compartmentalization, and parallelization. Multiplexing droplet content allows the investigation of various experimental conditions in a highly parallelized manner. Yet, droplet library generation and tracking remain challenging in high-throughput screening. The introduction of distinct reagents into droplets necessitates precise control over droplet flow in a microfluidic chip, limiting the throughput to a few reagents. Additionally, tracking individual droplets is complex due to their fast dynamics. To address these challenges, we have developed a multiplexing platform for automated sample preparation, enabling on-demand merging and mixing of reagents for fine-tuning the sample compositions for droplet generation. A coding space with 169 optical barcodes can be realized by the pairwise combination of four fluorescence dyes at six concentration levels to encode droplet populations as required by the experimental design. A machine-learning algorithm has been employed to identify distinct droplet populations. As proof of concept, we conducted an antibiotic susceptibility assay on an *E. coli* strain to screen for susceptibility of four antibiotics and determine minimum inhibitory concentrations in one experiment. Utilizing the on-demand sample preparation, optical barcodes, and machine-learning analysis, our setup provides a rapid, straightforward, and reliable multiplexing capability for numerous microbial and biochemical applications.

1. Introduction

Droplet-based microfluidics has been of great interest in the past decade due to several unique advantages. Using the technology, one can produce highly monodisperse droplets at thousands per second. The high generation rates make it a great approach for high-throughput and parallelized experimentations [1,2]. Droplets can have volumes ranging from pico- to nanoliter, reducing reagent consumption and cost for high-throughput applications. Also, the high surface area to volume ratio facilitates faster reaction times [3,4]. With these unique characteristics, droplet-based microfluidics has shown its potential in numerous high-throughput screening applications across various scientific and medical fields [5,6].

Droplets have also been extensively used for high-throughput screening in microbiological applications, including enzymatic activity [7–9], resistance to antibiotics [10–12], and combinatorial studies of drugs [13,14]. For such assays, it is often desired or necessary to investigate more than one experimental condition [15]. This simultaneously brings key advantages in the screening process, such as time efficiency, increased throughput, and reduced experimental variability. Desired conditions could be, for instance, different analyte concentrations, substrates, media compositions, or buffers. However, droplet library generation and content tracking are still critical challenges in high-throughput screening [16]. Multiplexing experimental conditions in a droplet-based microfluidic platform necessitates the development of complex process control, fluidic handling, and analysis pipelines due to reduced footprint and rapid sample transport within these platforms [17].

The introduction of distinct chemical compositions into droplets requires precise control over droplets flow within a microfluidic chip. This limits the reagents throughput that can be handled as the process dynamics need to be matched with droplet generation or reinjection. The rapid dynamics also make it a challenging process to track the droplet content back to its experimental condition. There have been

studies in this regard for combinatorial screening applications [10–12, 14,15,18–23]. In some of these approaches, a multiplexed sample preparation step is done prior to droplet generation, and then the prepared samples are fed into one or more microfluidic chips to make droplets. There are also gradient-based approaches [24], where different solutions are injected into the microfluidic chip using multiple inlets to produce droplets with different conditions. However, these methodologies would either require a labor-intensive process prior to droplet generation or precise flow control units as the reagent number rises. As a result, the sample preparation time and complexity will increase with new reagents being added for additional experimental conditions. Moreover, these approaches limit the combinatorial throughput and increase the chance for sample variability whilst sample reproducibility decreases (which is a big challenge in microbiological experimentation in general).

To reliably distinguish droplet contents within a library of different populations, various encoding strategies have been realized. In some optical barcoding strategies [14,21,22,25], certain concentrations of fluorescence dyes are used to encode different populations during the sample preparation step. Another optical barcoding method is the usage of colored or fluorescently labeled beads or quantum dots [18,26,27]. An alternative approach is nucleic acid-based barcoding that links to the genetic material within droplet content [28–30]. Although these approaches enable high-scale testing, they do not fully satisfy the needs, especially for on-demand combinatorial applications in microbiology. Also, in the case of nucleic acid-based barcoding, sequencing is required, which in turn necessitates droplet breaking and complex analysis procedures. Recently, an integrated microfluidic chip design has been developed that facilitates automated sample preparation for an antibiotic susceptibility assay [13] by employing a valve control layer. Using the integrated chip and four different drugs, they could test sixteen conditions. However, adding more reagent inlets will increase the design complexity and make the controlled merging and mixing of different reagents a challenging process. Moreover, droplets are tracked sequentially, which makes them prone to a disturbance within the chip. In this case, the applicability of the platform for microbiological applications is limited since no off-chip cultivation of larger droplet populations is possible.

In this work, we present a multiplexing platform for on-demand multiplexed sample preparation for combinatorial picolitre droplet generation through an automated sample plug generation, which directly feeds into the picolitre droplet generation. Sample plugs of up to 8 reagents can be efficiently merged and mixed prior to droplet generation to produce homogenous multiplexed populations. Importantly, as a single microfluidic chip is used, wash-plugs are introduced to ensure contamination-free droplet production. An optical barcoding strategy was employed to code the content of droplet populations using the combination of fluorescence dyes to generate up to 169 potential codes, which are decoded with machine learning methods. To demonstrate the applicability of the platform for microbiological applications, we performed a multiplexed antibiotic susceptibility assay with a library size of 25 different conditions for a model strain against four antibiotics. We demonstrated the susceptible antibiotics identification and determination of their minimum inhibitory concentrations in a single experimental run within 8 hours of incubation.

2. Materials and methods

2.1. Chip design and fluidic operations

The microfluidic chip designs were created using AutoCAD 2021 (Autodesk Corp., USA), and polydimethylsiloxane (PDMS) chips were fabricated by soft lithography[31]. A syringe pump (neMESYS, Cetoni) and Mitos Dropix (Dolomite) were used for fluidic operations. For plug and droplet generation, FC-40 (3 M) and Novel oil (HFE7500, 3 M) with 0.4 % fluorinated surfactant (FluoSurf, emulseo) were used.

2.2. Dye solution preparation for droplet encoding

All dye stocks were dissolved in DMSO. Alexa-Flour 647 (Thermo Fischer) at 6.4 and 32 μgmL^{-1} was used as two initial concentrations. Similarly, Alexa-Flour 488 (Thermo Fischer) at 8 μgmL^{-1}, Cascade-blue (Thermo Fischer) at 40 and 200 $mgmL^{-1}$, DY557 (Dyomics) at 0.8 and 4.4 $mgmL^{-1}$ were used for color coding. 6-Carboxyfluorescein (Sigma) at 1.6, 8, 0.8, and 4 $mgmL^{-1}$ were used as initial concentrations only for coding strategy demonstration. For the biological assays, the dye concentrations were premixed with cells or antibiotic solutions. Alexa-Flour 488 was used instead of 6-Carboxyfluorescein in biological experiments.

2.3. Bacterial sample preparation

The *E. coli* strain *ECJW922* [18] was used. As a culture medium, Terrific Broth (TB) with 1 % glucose was used. As seed culture, bacteria suspension from a Cryostock was inoculated in TB medium and incubated at 37°C, 180 rpm for ~20 h. For the main culture, TB medium was inoculated from the overnight culture with 0.1 OD600 and incubated at 37°C, 180 rpm for ~3 h until the culture reached an OD600 around 5. Aliquots of the main culture were prepared either at 0.048 or 0.06 OD600 as replicate one and two. This solution was loaded into the sample well stripe of the liquid handler. 2.5μL from this well is always taken for a 10-μL sample that will result a cell concentration around 2.4 and 3×10^6 cellsmL^{-1} for droplet generation of corresponding replicates (resulting in theoretical mean occupancy lambda=0.43 and 0.54 for 70-μm diameter droplets).

2.4. Antibiotic solution preparation

Stock concentrations of four antibiotics (premixed with dyes) were prepared before the experiment. The stock concentrations for nalidixic acid, kanamycin, tetracycline, and ciprofloxacin were 32, 32, 10, and 0.5 μgmL^{-1}, respectively.

2.5. Microscopy imaging

After droplet generation and 8 hours of incubation, droplets were imaged in the observation chamber. The chip was placed on an inverted microscope (Axio Observer Z1, Zeiss). Brightfield images were taken with a numerical aperture of 0.16 to intensify the cell edges for growth analysis. The Colibri 5 Zeiss was used as the light source for fluorescence images. Images were taken using 10× magnification and analyzed using a custom Python script (see supporting information section 7).

3. Results and discussion

3.1. Multiplexing platform set-up and operation

On-demand automated multiplexing of sample plugs for droplet generation is accomplished through three main steps (Steps 1–3), as illustrated in Fig. 1. In the first step, we used a commercial liquid handler (Mitos-Dropix Dolomite) to produce plugs with the desired volume. The liquid handler features an oil reservoir, a 24-sample-well stripe with the capacity to load up to 50 μL of reagent in each well, and a sample hook connected to a syringe pump. The sample hook moves between the wells and into each well defined by the device control software, and the desired plug volumes are withdrawn with defined oil spacing (Fig. 1). The minimum withdrawn volume depends on the working flow rate and inner diameter (ID) of the sample hook tubing. In our set-up, a tubing with 0.25 mm ID is used in the sample hook. This tubing is connected to a 1.5 mm ID tubing (Fig. 1) for plug storing and merging steps. In the second step, two or more plugs with different contents are merged. For two plugs with sufficiently close oil spacing, the transition from a narrow to a wider tubing configuration will result in merging. This is a known phenomenon happening in a
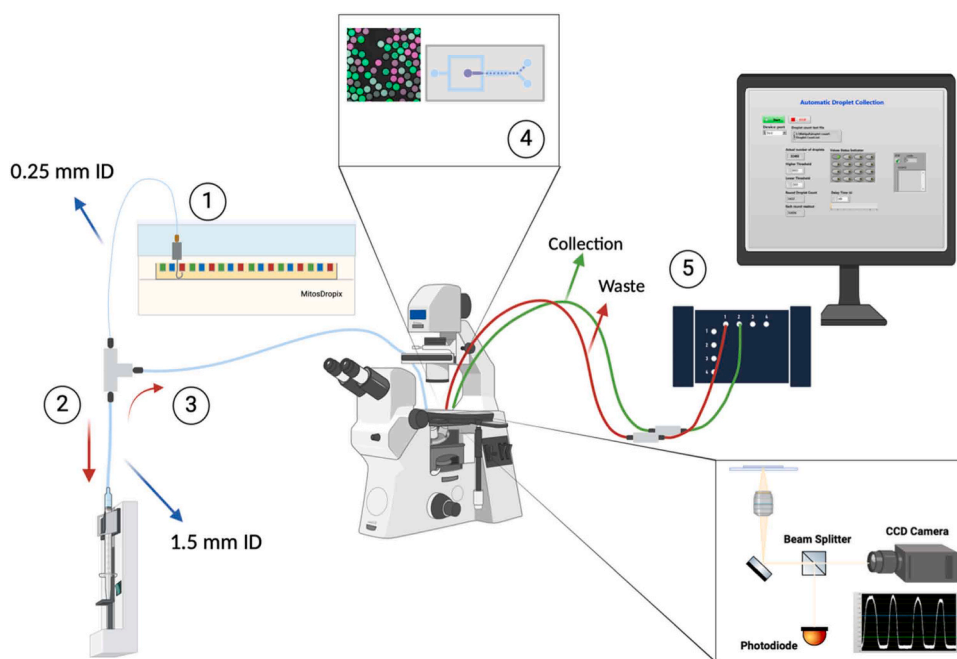
Fig. 1. Multiplexing platform workflow. Step 1: various reagents are loaded in the well stripe, and the commercial device is programmed to draw specific volumes from each well. Step 2: sample merging and storage: a transition from narrow tubing (ID = 0.25 mm) to wide tubing (ID = 1.5 mm) enables the merging of samples, and they are stored in the same tube. Step 3: Mixing via oscillatory flow: a 3-way valve connects the 1.5 mm tubing segments, and a syringe pump is programmed to create an oscillatory flow. Step 4: droplet generation: sample plugs are injected into microfluidic chip for droplet production. Step 5: To avoid the collection of droplets produced by wash-plugs, the chip outlet is automatically switched to ensure that only the desired droplets are collected.

microfluidic chip with expansion chambers[32]. We used a three-way valve in our platform to connect two tubings with different IDs (0.25 and 1.5 mm), as illustrated in Fig. 1. We optimized the platform to operate at 15 and 100 $\mu Lmin^{-1}$ based on the minimum oil spacing and the number of plugs that can be merged during the transition from small to wider tubing. We observed that for the higher flow rate, the oil spacing is large for merging. To solve this problem, in experiments with 100 $\mu Lmin^{-1}$, solutions were chemically modified by TWEEN20 to reduce the distance between the plugs as they flow inside the tubing [33]. Up to three plugs can be merged at 100 $\mu Lmin^{-1}$, while 8 plugs can be merged at 15 $\mu Lmin^{-1}$ (Table S1). For more details on the flow rate selection and sample preparation, see Figure S1 and supporting information sections 1 and 2. Similarly, the 1.5 mm tubing length was adjusted to assemble, mix, and store at least 7 final sample plugs for a multiplexing experiment with up to 14 conditions.

In step three, the merged plugs are mixed to obtain a homogenous mixture within the final sample plug, resulting in a uniform droplet population. The 3-way valve is switched to connect the two 1.5 mm tubing segments to perform the mixing via oscillatory segmented flow generated through a programmed syringe pump (Fig. 2a). In this approach, two axisymmetric recirculation zones are formed inside the liquid plug to enhance the mixing of the solute molecules [34]. We have investigated the mixing efficiency for 10-μL plugs (merged plugs of phosphate buffer saline (PBS) and *6-carboxyfluorescein* at different ratios) by analyzing the variation in the mean intensity of the subsequently generated droplet population. Four different concentrations were made each having four plug replicates. We used 1000 cycles of 500 ms for mixing the samples with a flow rate of 1000 $\mu Lmin^{-1}$. The plug volume has an impact on the length of the plug and the required number of mixing cycles: the lower the volume, the faster the mixing process. Also, the reagent's properties, such as density, viscosity, and hydrophobicity, play an important role in defining the necessary cycle number for mixing. Fig. 2b shows the droplet populations intensity histogram generated from 10-μL sample plugs utilizing an optimized chip design (see supporting information section 3; Figs. S2–3). The average variation in the

green fluorescence intensity of droplets is below 10 %, which signifies an efficient mixing within a 10-μL plug using the defined mixing parameters. After mixing, samples are used for droplet generation (step 4 in Fig. 1, Fig. 2c-d).

3.2. Prevention of cross-contamination and automated droplet collection

In our platform, we are using a single microfluidic chip for droplet generation from multiple conditions. During the transport in the channel, reagent residue can be left behind by the previous sample, which can contaminate the subsequent sample. Thus, cross-contamination must be avoided and minimized as it can lead to imprecise assay outcomes. To investigate the cross-contamination possibility in our platform, we generated a two-member droplet library of PBS sample plugs color-coded with red and green fluorescence dyes. In the scatter plot, there are droplets with intermediate intensities showing contamination from the other dye (Fig. 3a). In a second experiment, we introduced a wash-plug of pure PBS between the samples aiming to clean the microfluidic chip. These wash-plugs significantly reduced the cross-contamination (Fig. 3b). However, while wash-plugs clean the chip, they also produce undesired droplets. To avoid these droplets, we developed an automatic droplet collection set-up (Step 5 in Fig. 1).

The set-up uses an optical counter[35] on the observation microscope during droplet generation alongside an electromagnetic valve (Multiplexer flow matrix, Elveflow) controlling the outlets of the microfluidic chip. Using the set-up, a custom-written LabVIEW software switches between the collection and waste outlets using three parameters: time-spacing between the main samples, the lower and upper counter thresholds. Working flow rate defines time-spacing. The upper and lower counter thresholds define the number of droplets to be ignored initially and collected, respectively, and are dependent on the sample volume and the target size of each droplet population.

In our experiments, we generated several 10-μL final sample plugs, and at 15 $\mu Lmin^{-1}$, the time-spacing is around 75 seconds. After droplet generation, we ignored all wash-plug droplets and the first 2000
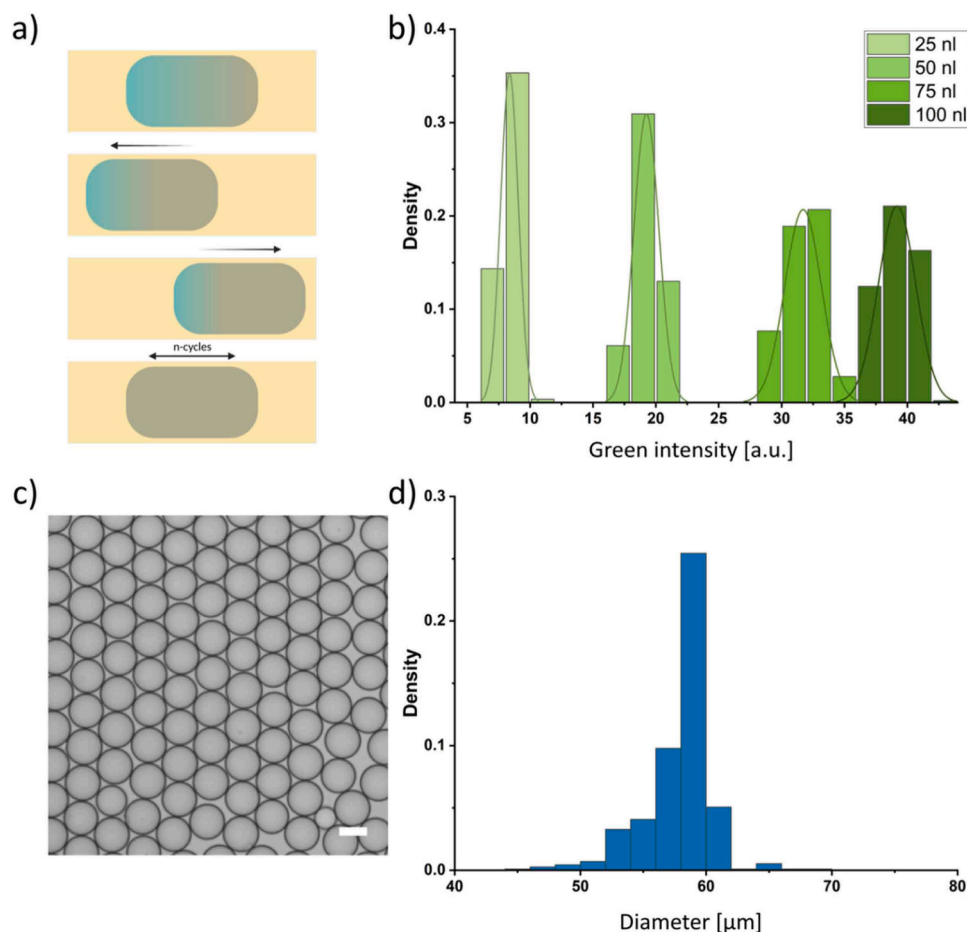
Fig. 2. (a) Schematic of mixing process within the tubing. The oscillatory fluid flow generated by programming the syringe pump promotes the mixing. (b) Green fluorescence intensities from four distinct droplet populations generated from the mixed plugs exhibited an average coefficient of variation of 6.15 %, indicating an effective mixing (n= 5223). (c) Brightfield image of droplets generated from a 2-μL sample (scale bar = 50 μm). (d) Distribution of droplet diameters, indicating monodisperse population produced by the optimized chip with a CV = 4.98 % (n =562).

droplets of each sample. Then, we collected between 45 and 60 thousand droplets per sample (see supporting information section 4). Fig. 3d shows the intensity scatter plot of the two-member droplet library using the automated collection of droplets. This result indicates that the automated collection of droplets can successfully collect the desired droplets with a 99.96 % efficiency.

3.3. Droplet encoding and decoding

In previous applications with limited library size and throughput [13], sample droplets are typically temporally encoded in an integrated chip design so that the analysis sequence identifies the different experimental conditions. Conversely, multiplexed droplets collection for off-chip incubation, which is a central aspect of all our microbiological applications, will change the order of droplets and make it impossible to analyze the assay for different conditions. Thus, it is essential to implement proper coding strategies to take advantage of the full capacity of high-throughput droplet microfluidics. To encode the multiplexed droplet populations, four fluorescence dyes were used: Red, Green, Far-red, and Blue. For each dye, we have chosen two different initial stock concentrations, with the 'higher' concentration set at least five times higher than the 'lower'. From each stock concentration loaded in wells of the liquid sampler, we produced 10-μL plugs of three sub-concentrations (0.25X, 0.5X, 0.75X) of the initial dye concentrations by merging and mixing with other plugs as described above. The concentrations were carefully selected so that for a fixed camera exposure time and light source excitation power, the final six intensities lie within

the detection limit and are distinguishable in an 8 or 16-bit image. Using four dyes and only the single-color shade, we can produce a 24-member (4 dyes X 6 concentrations) library.

Next, we generated 10-μL final samples with every pairwise combination of two dyes at the three sub-concentrations. Using this approach and a fixed sample volume of 10-μL, 24 (see Figure S4 and supporting information section 5 for detailed calculations) and 144 codes with four dyes at pairwise combination (6×24 codes) can be realized.

To establish the decoding pipeline, 24 pairwise combinations for each pair of dyes were generated and collected separately. Droplets were imaged in their corresponding fluorescence channels (Fig. 4a). Using a Python script (see supporting information section 7), droplets were identified in every image, and the mean intensity for every single droplet was measured to identify individual droplet populations. Figure S5 shows the intensity histogram for every dye for two stock concentrations. To identify the different droplet populations, we used density-based spatial clustering of applications with noise (DBSCAN) [36]. DBSCAN will identify the dense regions or clusters within every combination and eliminate the noise from the droplet library (Fig. 4b). The noise sources in our experiments are due to droplet fusion or splitting during transport. These sources cause either shifts from the cluster center or mixed intensity populations that are contrary to the color code construction. We could achieve 144 fluorescence codes using pair-wise combinations of single-color intensities plus one population without fluorescence dye. Adding the single-color pallet (Figure S5) will increase the coding possibility to 169 fluorescence barcodes.

However, DBSCAN becomes unreliable once the distance between
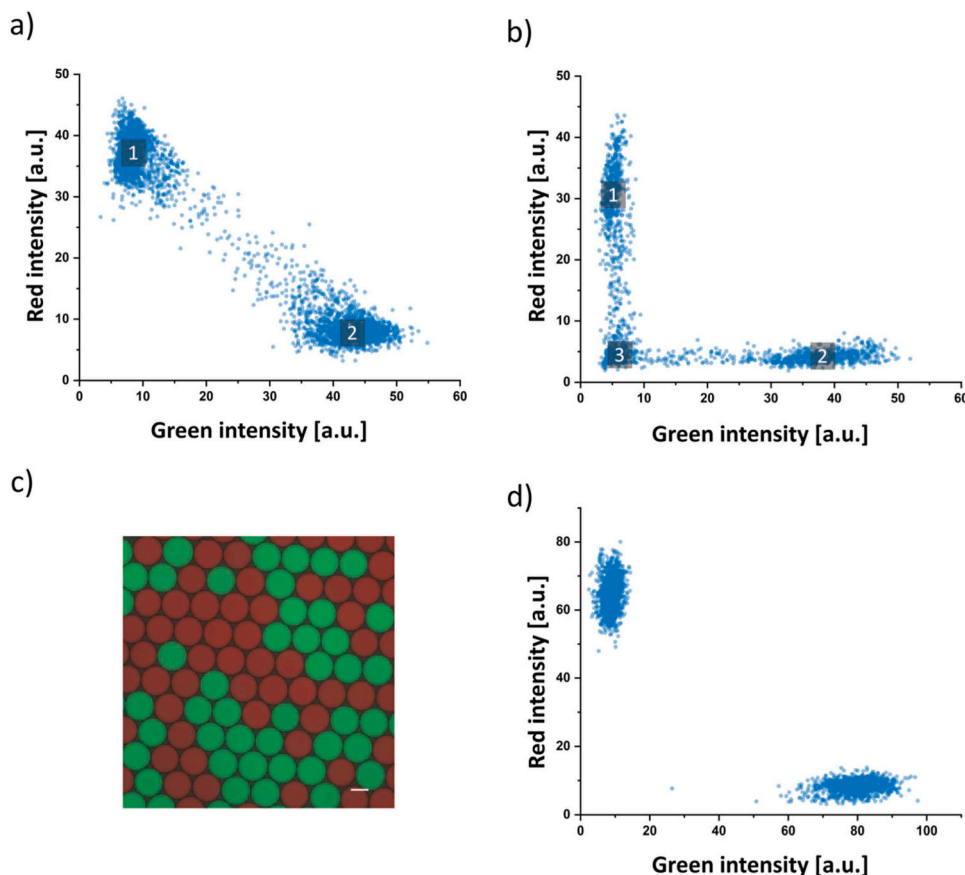
Fig. 3. (a) Scatter plot representing two droplet populations generated consecutively through the microfluidic chip (n = 3104). The residual contamination from the previous sample impacts the subsequent droplet generation, resulting in contamination with both fluorescent dyes. (b) The introduction of wash-plugs between each sample reduces the cross-contamination by cleaning the chip; however, intermediate droplets (cloud 3) are still collected (n = 1757). (c) The overlayed fluorescence and brightfield image of a two-member droplet library, collected using the automated droplet collection set-up. (d) Scatter plot of droplets collected by employing the automated droplet collection segment, which eliminates the collection of intermediate droplets with an accuracy of 99.96 % (n = 2415).

clusters differs. As in our case, for the lowest initial dye concentration, clusters are closer together than for the highest. This requires multiple DBSCAN rounds, and fine-tuning algorithm parameters to identify all clusters each time. Moreover, if fewer droplets are present for a certain condition, the DBSCAN may overlook that condition due to a smaller sample size. To avoid these efforts for each experiment and to have a robust analysis pipeline, we have developed a machine learning model (see supporting information section 7). The model is trained using the DBSCAN clustering results and identifies the conditions in two steps. First, it identifies the color combinations, and second, the color-codes used for each combination. To show the applicability of the model, we prepared a library of 24 fluorescence codes by mixing droplets of blue-far-red and green-red combinations (Fig. 5a). Using the model, the color combinations are identified, and the used optical codes are detected. Figure S6 shows the confusion matrix of the model for identification of the combinations at an accuracy of more than 99.7 % (Table S2). In Fig. 5b, using t-distributed stochastic neighbor embedding (t-SNE), fluorescence barcodes in the 24-member library are visualized in a 2D scatter plot.

It should be emphasized that the 169 fluorescence barcodes is the available coding space to choose from for an experiment, which can be restricted by fluorescence channels being required for the assay [5,37]. Therefore, a reasonable final library size will be determined by the assay requirements. Even with two coding-colors, library sizes of 24–36 members are possible. The four-color coding set-up allows the user to choose the best colors with the least interference with assay measurements.

Besides the coding space, the time required to compose the target

library is a critical factor, which is determined by the operation flow rate and the number of reagents required for library preparation. In our experiments, we have used 15 μLmin^{-1} as the operating flow rate. At this flow rate, we can merge up to eight reagents, which results in around one hour of operation time for 12 conditions (Fig. 1 steps 1–5, Table S1). However, if fewer reagents are required, we can use faster flow rates, resulting in lower preparation times. Table S1 shows the required preparation time for 12 multiplexed samples with different flow rates for the range of available reagents. We also calculated the maximum droplet library size that could be prepared in 2 hours at the different flow rates to provide an overview of the technology's capacity for experiments where the microbial inoculum is used, i.e., sample preparation should be faster than the lag-phase of the microbial growth. The range lies between 27 conditions at 15 μLmin^{-1} and 42 conditions at 100 μLmin^{-1}. Additionally, if necessary, multiplexed droplet populations can be produced without the time-sensitive biological/chemical sample. The biological/chemical sample can be later introduced to each droplet by pico-injection at a high frequency (1 kHz) [38]. Moreover, the presented coding strategy enables the integration of the droplet library to various analysis techniques, such as fluorescence-activated droplet sorting [7, 39], mass-spectrometry [40], fluorescence microscopy, and optical spectroscopy approaches.

3.4. Antibiotic susceptibility assay

To validate the applicability of the multiplexing platform, we performed an antibiotic susceptibility assay with an *E. coli JW992* strain against four antibiotics. This strain has been well studied for its
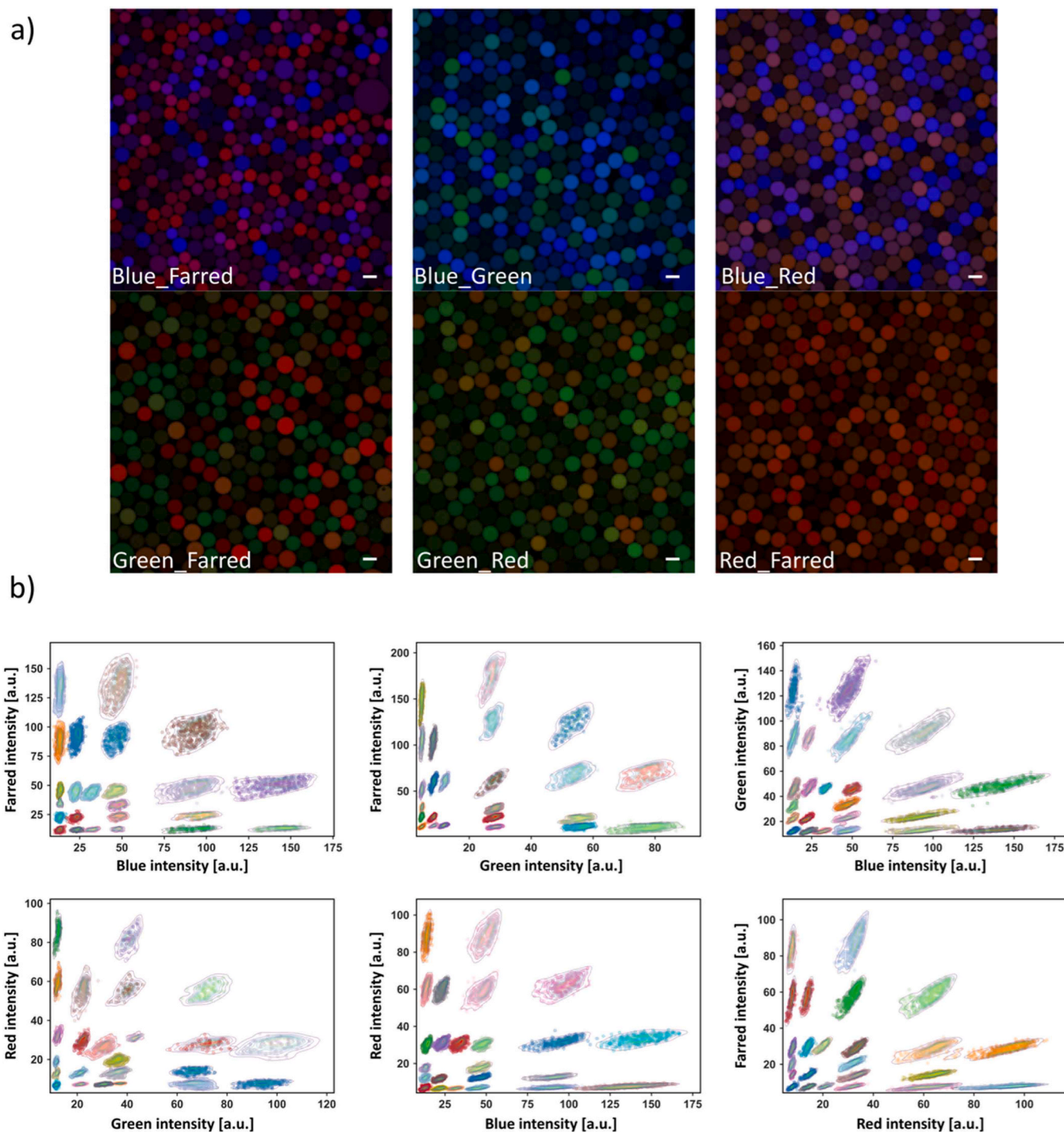
Fig. 4. (a) Fluorescence images of each pairwise combination containing 24 color codes. To identify barcoded droplet populations, intensities of the raw data from each color-code combination are extracted (at least 4078 droplets per pairwise combination) and analyzed using DBSCAN, which is visualized here as 2D scatter plots in (b) representing individual color-coded populations within every pairwise library. The contours derived from kernel density estimation indicate the density distribution of each cluster.

susceptibility in our previous work [18]. We included tetracycline hydrochloride (TET), ciprofloxacin hydrochloride (CIP), kanamycin sulfate (KAN), and nalidixic acid (NA), knowing that this *E. coli* is susceptible to two of these compounds (TET and CIP) within the tested range. We produced a 25-member library of 10-µL plugs in two runs (total assembly time ~2 hours).

Using the platform, bacterial cells were encapsulated with six concentrations of each antibiotic from one stock concentration. Also, one control population without antibiotics was produced. After supervised

droplet generation, the droplet library was dynamically incubated for 8 hours [41], and a sub-sample of droplets was imaged for growth analysis and decoding (see supporting information section 7 for more detail).

Using the analysis pipeline, we could automatically identify the color codes (Fig. 6c-d). Accordingly, we analyzed the growth inside every droplet of each population (see supporting information section 7). The growth analysis scatter plot (Figure S7) in the control population indicates two separate populations: empty and growth-exhibiting
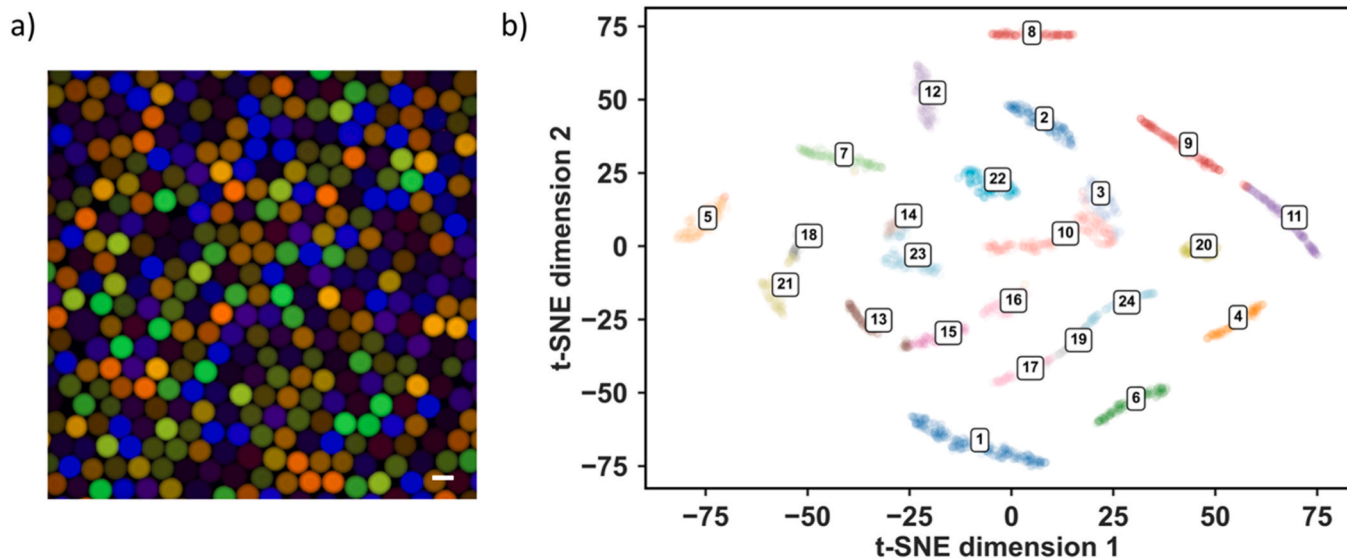
Fig. 5. (a) Fluorescence image of a 24-member droplet library (scale bar = 100 µm). 12 codes from each of the blue-far-red and green-red combinations were mixed. A machine learning model based on a K-neighbors classifier is developed to identify combinations and their corresponding color codes with more than 99.7 % accuracy. (b) Showing the t-SNE plot of the identified 24 populations (labeled: 1–24) within the library (n = 3785).
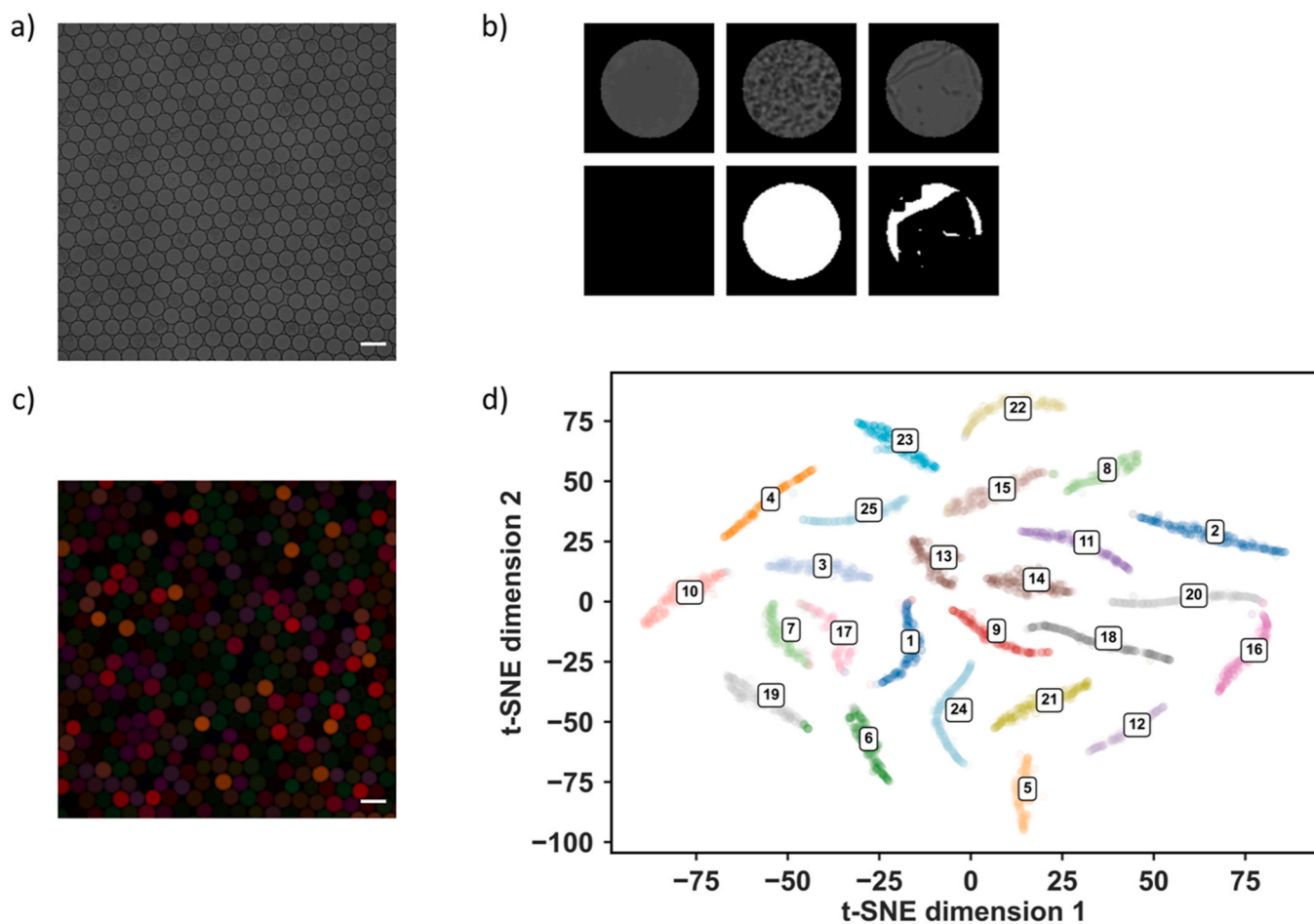

Fig. 6. An antibiotic susceptibility assay for *E. coli* was designed to investigate the platform's applicability in microbiological applications. In (a), the brightfield image (after incubation) is utilized in the analysis pipeline for growth quantification. (b) Represents the original image of three exemplary droplets (top) alongside the final binary image (bottom) that have undergone image processing steps. Growth is quantified by measuring the area of the white pixels and normalizing it to the droplet area. (c) Shows the merged fluorescence image in four channels that are used color code identification within the experiment. Using the machine learning model, 25 color codes are identified, and t-SNE plot is presented in (d) for one biological replicate (n = 7533 droplets).

droplets. Using this information, we set a threshold (= 15, see supporting information section 7) on the growth analysis values to identify growth-exhibiting droplets in other populations. We then introduced the growth score as the mean growth of a population considering the droplet occupancy to have an accurate growth analysis (see supporting information section 7). Fig. 7a-d show the histogram of the normalized growth score for each antibiotic.

We defined susceptible antibiotics to result in over 95 % reduction of the normalized growth score (Figure S8) when comparing the highest antibiotic concentration to the control. This classification is necessary for MIC calculations as they are only valid for susceptible antibiotics. Next, the normalized growth score bar plots were analyzed to determine the MIC by fitting a nonlinear dose-response curve. With this

information, MICs were determined for TET and CIP to be 1.01 and 0.11 µgmL^{-1}, respectively (Fig. 7e-f, Table S3), with the MIC criteria set to a 95 % reduction in the growth score of the fitted curve. The MIC fits within the MIC quality range (2-fold dilution range from MIC) determined using a traditional microtiter plate experiment (0.0625 µgml^{-1} for CIP (Figs. S9) and 2 µgml^{-1} for TET [18]), which validates the method for determining the MIC.

It has been shown that depending on the physiochemical properties of the antibiotic, antibiotic concentration, and droplets distance, antibiotics may leak between droplets [42]. Therefore, it is necessary to identify the properties of all antibiotics beforehand and utilize proper control conditions in the experiment to ensure precise assay outcomes. For our strain, no inhibition in the control population was observed, and
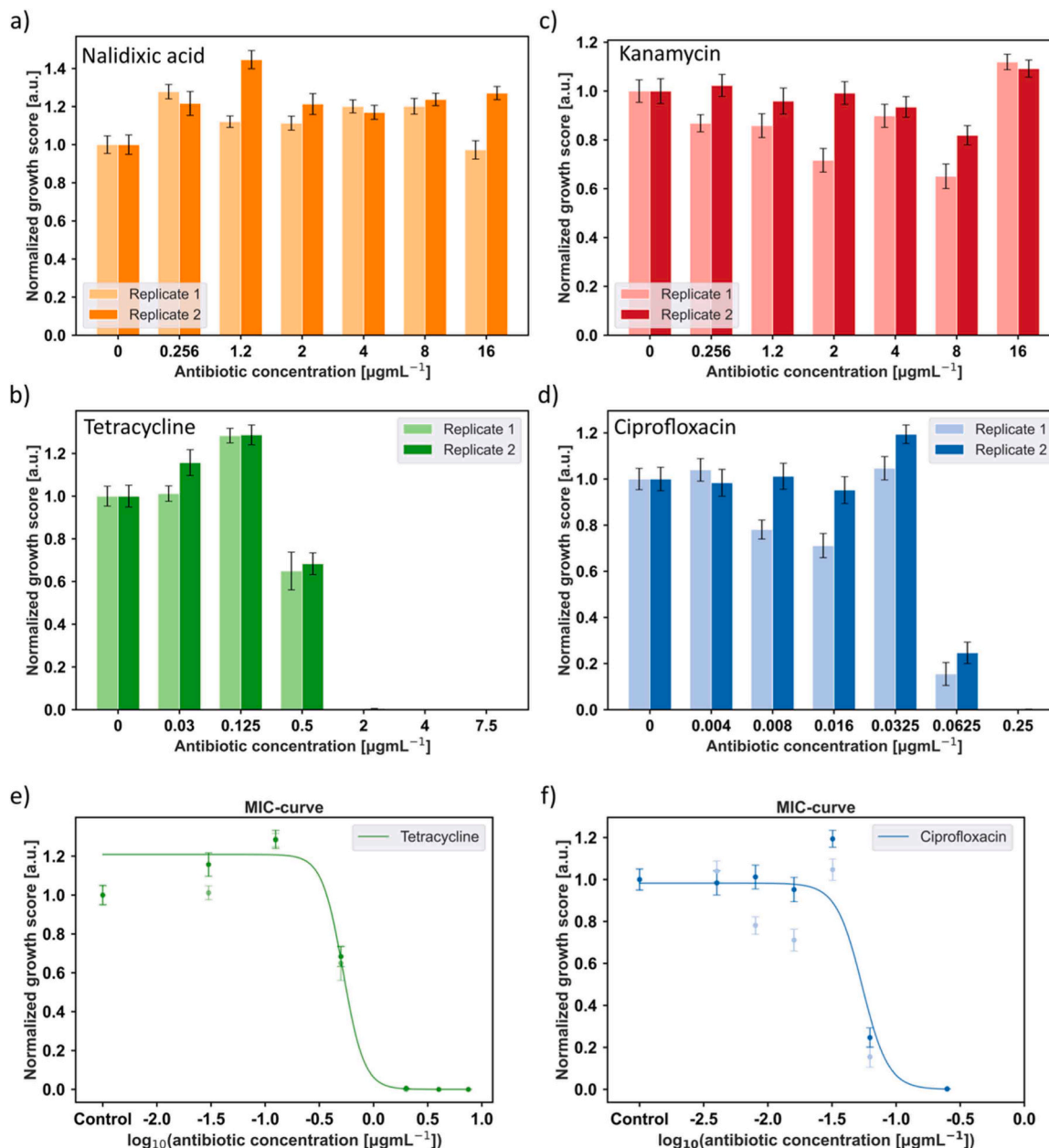

Fig. 7. Growth within each droplet of different color-codes is quantified through the analysis pipeline. To account for the analysis of a small sample size within a large library population (7533 or 14,084 out of nearly 1 million droplets in replicate 1 and 2, respectively), the growth score is introduced to normalize the effect for every condition. (a), (b), (c), and (d) show bar plots of normalized growth scores for the two biological replicates of *E. coli* cultivations with different concentrations of Nalidixic acid, Kanamycin, Tetracycline, and Ciprofloxacin, respectively. In (e) and (f), sigmoidal fit results of two biological replicates of Ciprofloxacin and Tetracycline are shown, respectively. A 95 % reduction in the fitted curve is considered the minimum inhibitory concentration for each antibiotic, with values of 1.01 and 0.11 µgmL^{-1} for Tetracycline and Ciprofloxacin, respectively. Error bars represent the standard error in the mean.

the MIC results were reliable. For this experiment, we consider possible leakage effects irrelevant, but validating this is crucial for every operation. The reported assay underscores the capabilities of the platform from multiplexing experimental conditions to analysis of the complex datasets with profound implications for advanced microbiological experimentations.

4. Conclusions

We present a platform for on-demand multiplexed sample preparation in an automated manner. Cross-contamination-free mono-disperse picolitre droplet libraries were realized using the platform from sample plug volumes ranging from 2 to 10 µl. We have developed a flexible coding space with up to 169 optical barcodes to simultaneously study different experimental conditions in droplet-based microfluidics. A robust de-coding machine learning model was developed to effectively identify the color codes within a droplet library. Furthermore, the platform was successfully demonstrated to perform an antibiotic susceptibility assay and determine MIC concentrations with *E. coli* as a model strain.

In our experiments, microscopy was the measurement approach of droplet content. This means we only sample a small portion of the droplet library to evaluate the experimental conditions. However, we also developed an optofluidic measurement technique[39,43] to analyze the droplet content at high-speed inflow (up to 1 kHz). Integrating the platform into this technology will significantly increase the accuracy of analysis by increasing the analysis throughput. However, the data analysis of many conditions, especially when coupled with brightfield image analysis for growth, is still challenging and is only possible at a slower rate. In our future work, we aim to integrate the platform with optofluidic measurements and enable real-time data analysis. Also, to improve the time throughput for droplet generation, multiple Mitos units or smaller final plugs can be used depending on the microbiological needs. In addition, the tubing length can be increased to maximize the number of plugs stored and mixed. We envision the presented platform will become a significant approach for microbiological applications, including combinatorial drug discovery, antibiotic resistance studies, assay optimization, and novel natural product screening, by integrating various experimental conditions in droplet cultivation experiments. For instance, microbial communities from a natural environment can be simultaneously assessed in various conditions, e.g., growth media, and certain microbial communities can be selected and screened for novel natural products. Moreover, metagenomic approaches enable profiling the functional potential of these communities. Therefore, the platform enhances the capabilities of microbiological research in understanding the functional diversity of the microbial world.

CRediT authorship contribution statement

Ashkan Samimi: Writing – original draft, Visualization, Validation, Software, Methodology, Investigation, Formal analysis, Data curation, Conceptualization. **Sundar Hengoju:** Writing – review & editing, Validation, Methodology, Conceptualization. **Miriam Rosenbaum:** Writing – review & editing, Supervision, Project administration, Funding acquisition, Conceptualization.

Declaration of Competing Interest

The authors declare that they have no known competing financial interests or personal relationships that could have appeared to influence the work reported in this paper.

Data availability

The data that supports the findings of this study is available from the corresponding author upon reasonable request.

Appendix A. Supporting information

Supplementary data associated with this article can be found in the online version at doi:10.1016/j.snb.2024.136162.

References

[1] L. Mahler, S.P. Niehs, K. Martin, T. Weber, K. Scherlach, C. Hertweck, M. Roth, M. A. Rosenbaum, Highly parallelized droplet cultivation and prioritization on antibiotic producers from natural microbial communities, Elife 10 (2021), https://doi.org/10.7554/ELIFE.64774.

[2] M. Najah, A.D. Griffiths, M. Ryckelynck, Teaching single-cell digital analysis using droplet-based microfluidics, Anal. Chem. 84 (2012) 1202–1209, https://doi.org/10.1021/ac202645m.

[3] S.Y. Teh, R. Lin, L.H. Hung, A.P. Lee, Droplet microfluidics, Lab Chip 8 (2008) 198–220, https://doi.org/10.1039/b715524g.

[4] M.T. Guo, A. Rotem, J.A. Heyman, D.A. Weitz, Droplet microfluidics for high-throughput biological assays, Lab Chip 12 (2012) 2146–2155, https://doi.org/10.1039/c2lc21147e.

[5] L. Mahler, K. Wink, R.J. Beulig, K. Scherlach, M. Tovar, E. Zang, K. Martin, C. Hertweck, D. Belder, M. Roth, Detection of antibiotics synthetized in microfluidic picolitre droplets by various actinobacteria, Sci. Rep. 8 (2018) 1–11, https://doi.org/10.1038/s41598-018-31263-2.

[6] R. Tu, Y. Zhang, E. Hua, L. Bai, H. Huang, K. Yun, M. Wang, Droplet-based microfluidic platform for high-throughput screening of Streptomyces, Commun. Biol. 4 (2021) 1–9, https://doi.org/10.1038/s42003-021-02186-y.

[7] D.A. Holland-Moritz, M.K. Wismer, B.F. Mann, I. Farasat, P. Devine, E. D. Guetschow, I. Mangion, C.J. Welch, J.C. Moore, S. Sun, R.T. Kennedy, Mass Activated Droplet Sorting (MADS) Enables High-Throughput Screening of Enzymatic Reactions at Nanoliter Scale, Angew. Chem. Int. Ed. 59 (2020) 4470–4477, https://doi.org/10.1002/anie.201913203.

[8] X.D. Zhu, X. Shi, S.W. Wang, J. Chu, W.H. Zhu, B.C. Ye, P. Zuo, Y.H. Wang, High-throughput screening of high lactic acid-producing Bacillus coagulans by droplet microfluidic based flow cytometry with fluorescence activated cell sorting, RSC Adv. 9 (2019) 4507–4513, https://doi.org/10.1039/C8RA09684H.

[9] S.L. Sjostrom, Y. Bai, M. Huang, Z. Liu, J. Nielsen, H.N. Joensson, H. Andersson Svahn, High-throughput screening for industrial enzyme production hosts by droplet microfluidics, Lab Chip 14 (2014) 806–813, https://doi.org/10.1039/c3lc51202a.

[10] K. Churski, T.S. Kaminski, S. Jakiela, W. Kamysz, W. Baranska-Rybak, D.B. Weibel, P. Garstecki, Rapid screening of antibiotic toxicity in an automated microdroplet system, Lab Chip 12 (2012) 1629–1637, https://doi.org/10.1039/c2lc21284f.

[11] P. Zhang, A.M. Kaushik, K. Hsieh, S. Li, S. Lewis, K.E. Mach, J.C. Liao, K.C. Carroll, T. Wang, A Cascaded Droplet Microfluidic Platform Enables High-Throughput Single Cell Antibiotic Susceptibility Testing at Scale, 2101254 (2022) 1–12. https://doi.org/10.1002/smtd.202101254.

[12] W. Kang, S. Sarkar, Z.S. Lin, S. McKenney, T. Konry, Ultrafast parallelized microfluidic platform for antimicrobial susceptibility testing of gram positive and negative bacteria, Anal. Chem. 91 (2019) 6242–6249, https://doi.org/10.1021/acs.analchem.9b00939.

[13] H. Li, P. Zhang, K. Hsieh, T.-H. Wang, Combinatorial nanodroplet platform for screening antibiotic combinations, Lab Chip (2022), https://doi.org/10.1039/d1lc00865j.

[14] A. Kulesa, J. Kehe, J.E. Hurtado, P. Tawde, P.C. Blainey, Combinatorial drug discovery in nanoliter droplets, Proc. Natl. Acad. Sci. 115 (2018) 6685–6690, https://doi.org/10.1073/pnas.1802233115.

[15] J. Kehe, A. Kulesa, A. Ortiz, C.M. Ackerman, S.G. Thakku, D. Sellers, S. Kuehn, J. Gore, J. Friedman, P.C. Blainey, Massively parallel screening of synthetic microbial communities, Proc. Natl. Acad. Sci. U. S. A. 116 (2019) 12804–12809, https://doi.org/10.1073/pnas.1900102116.

[16] E.M. Payne, D.A. Holland-Moritz, S. Sun, R.T. Kennedy, High-throughput screening by droplet microfluidics: perspective into key challenges and future prospects, Lab Chip 20 (2020) 2247–2262, https://doi.org/10.1039/d0lc00347f.

[17] Y. Ding, P.D. Howes, A.J. Demello, Recent advances in droplet microfluidics, Anal. Chem. 92 (2020) 132–149, https://doi.org/10.1021/acs.analchem.9b05047.

[18] C.M. Svensson, O. Shvydkiv, S. Dietrich, L. Mahler, T. Weber, M. Choudhary, M. Tovar, M.T. Figge, M. Roth, Coding of Experimental Conditions in Microfluidic Droplet Assays Using Colored Beads and Machine Learning Supported Image Analysis, Small 15 (2019) 1–14, https://doi.org/10.1002/smll.201802384.

[19] W. Postek, P. Gargulinski, O. Scheler, T.S. Kaminski, P. Garstecki, Microfluidic screening of antibiotic susceptibility at a single-cell level shows the inoculum effect of cefotaxime on: E. coli, Lab Chip 18 (2018) 3668–3677, https://doi.org/10.1039/c8lc00916c.

[20] S.N. Agnihotri, M.R. Raveshi, R. Bhardwaj, A. Neild, Microvalves for integrated selective droplet generation, splitting and merging on a chip, Microfluid. Nanofluidics 25 (2021) 1–13, https://doi.org/10.1007/s10404-021-02487-y.

[21] J.Q. Zhang, C.A. Siltanen, A. Dolatmoradi, C. Sun, K.-C. Chang, R.H. Cole, Z. J. Gartner, A.R. Abate, High diversity droplet microfluidic libraries generated with a commercial liquid spotter, Sci. Rep. 11 (2021) 4351, https://doi.org/10.1038/s41598-021-83865-y.

[22] C.M. Ackerman, C. Myhrvold, S.G. Thakku, C.A. Freije, H.C. Metsky, D.K. Yang, S. H. Ye, C.K. Boehm, T.S.F. Kosoko-Thoroddsen, J. Kehe, T.G. Nguyen, A. Carter, A. Kulesa, J.R. Barnes, V.G. Dugan, D.T. Hung, P.C. Blainey, P.C. Sabeti, Massively multiplexed nucleic acid detection with Cas13, Nature 582 (2020) 277–282, https://doi.org/10.1038/s41586-020-2279-8.

[23] D. Cai, Y. Wang, J. Zou, Z. Li, E. Huang, X. Ouyang, Z. Que, Y. Luo, Z. Chen, Y. Jiang, G. Zhang, H. Wu, D. Liu, Droplet encoding-pairing enabled multiplexed digital loop-mediated isothermal amplification for simultaneous quantitative detection of multiple pathogens, Adv. Sci. 2205863 (2023) 1–11, https://doi.org/10.1002/advs.202205863.

[24] Y. Hori, C. Kantak, R.M. Murray, A.R. Abate, Cell-free extract based optimization of biomolecular circuits with droplet microfluidics, Lab Chip 17 (2017) 3037–3042, https://doi.org/10.1039/c7lc00552k.

[25] A. Baccouche, S. Okumura, R. Sieskind, E. Henry, N. Aubert-Kato, N. Bredeche, J. F. Bartolo, V. Taly, Y. Rondelez, T. Fujii, A.J. Genot, Massively parallel and multiparameter titration of biochemical assays with droplet microfluidics, Nat. Protoc. 12 (2017) 1912–1932, https://doi.org/10.1038/nprot.2017.092.

[26] G.K. Zath, R.A. Sperling, C.W. Hoffman, D.A. Bikos, R. Ablacci, A.R. Abate, D. A. Weitz, C.B. Chang, Rapid parallel generation of a fluorescently barcoded drop library from a microtiter plate using the plate-interfacing parallel encapsulation (PIPE) chip, Lab Chip (2022) 4735–4745, https://doi.org/10.1039/d2lc00909a.

[27] H.Q. Nguyen, B.C. Baxter, K. Brower, C.A. Diaz-Botia, J.L. DeRisi, P.M. Fordyce, K. S. Thorn, Programmable microfluidic synthesis of over one thousand uniquely identifiable spectral codes, Adv. Opt. Mater. 5 (2017) 1–6, https://doi.org/10.1002/adom.201600548.

[28] X.D. Zhu, X. Shi, S.W. Wang, J. Chu, W.H. Zhu, B.C. Ye, P. Zuo, Y.H. Wang, High-throughput screening of high lactic acid-producing Bacillus coagulans by droplet microfluidic based flow cytometry with fluorescence activated cell sorting, RSC Adv. 9 (2019) 4507–4513, https://doi.org/10.1039/C8RA09684H.

[29] F. Lan, J.R. Haliburton, A. Yuan, A.R. Abate, Droplet barcoding for massively parallel single-molecule deep sequencing, Nat. Commun. 7 (2016) 1–10, https://doi.org/10.1038/ncomms11784.

[30] A.M. Klein, L. Mazutis, I. Akartuna, N. Tallapragada, A. Veres, V. Li, L. Peshkin, D. A. Weitz, M.W. Kirschner, Droplet barcoding for single-cell transcriptomics applied to embryonic stem cells, Cell 161 (2015) 1187–1201, https://doi.org/10.1016/j.cell.2015.04.044.

[31] M. Tovar, T. Weber, S. Hengoju, A. Lovera, A.S. Munser, O. Shvydkiv, M. Roth, 3D-glass molds for facile production of complex droplet microfluidic chips, Biomicrofluidics 12 (2018), https://doi.org/10.1063/1.5013325.

[32] K. Liu, H. Ding, Y. Chen, X.Z. Zhao, Droplet-based synthetic method using microflow focusing and droplet fusion, Microfluid. Nanofluidics 3 (2007) 239–243, https://doi.org/10.1007/s10404-006-0121-8.

[33] D. Ferraro, M. Serra, D. Filippi, L. Zago, E. Guglielmin, M. Pierno, S. Descroix, J. L. Viovy, G. Mistura, Controlling the distance of highly confined droplets in a capillary by interfacial tension for merging on-demand, Lab Chip 19 (2019) 136–146, https://doi.org/10.1039/c8lc01182f.

[34] M. Abolhasani, A. Oskooei, A. Klinkova, E. Kumacheva, A. Günther, Shaken, and stirred: oscillatory segmented flow for controlled size-evolution of colloidal nanomaterials, Lab Chip 14 (2014) 2309–2318, https://doi.org/10.1039/c4lc00131a.

[35] E. Zang, S. Brandes, M. Tovar, K. Martin, F. Mech, P. Horbert, T. Henkel, M. T. Figge, M. Roth, Real-time image processing for label-free enrichment of Actinobacteria cultivated in picolitre droplets, Lab Chip 13 (2013) 3707–3713, https://doi.org/10.1039/c3lc50572c.

[36] M. Ester, H.-P. Kriegel, J. Sander, X. Xu, A Density-Based Algorithm for Discovering Clusters in Large Spatial Databases with Noise, in: Proceedings of the Second Int. Conf. Knowl. Discov. Data Min., 1996: 226–231. https://doi.org/10.11901/1005.3093.2016.318.

[37] A.M. Kaushik, K. Hsieh, L. Chen, D.J. Shin, J.C. Liao, T.H. Wang, Accelerating bacterial growth detection and antimicrobial susceptibility assessment in integrated picoliter droplet platform, Biosens. Bioelectron. 97 (2017) 260–266, https://doi.org/10.1016/j.bios.2017.06.006.

[38] A.R. Abate, T. Hung, P. Marya, J.J. Agresti, D.A. Weitz, High-throughput injection with microfluidics using picoinjectors using picoinjectors, Proc. Natl. Acad. Sci. U. S. A. 107 (2010) 19163–19166, https://doi.org/10.1073/pnas.1006888107.

[39] M. Tovar, S. Hengoju, T. Weber, L. Mahler, M. Choudhary, T. Becker, M. Roth, One sensor for multiple colors: fluorescence analysis of microdroplets in microbiological screenings by frequency-division multiplexing, Anal. Chem. (2019), https://doi.org/10.1021/ACS.ANALCHEM.8B05451/SUPPL_FILE/AC8B05451_SI_001.PDF.

[40] K. Wink, L. Mahler, J.R. Beulig, S.K. Piendl, M. Roth, D. Belder, An integrated chip-mass spectrometry and epifluorescence approach for online monitoring of bioactive metabolites from incubated Actinobacteria in picoliter droplets, Anal. Bioanal. Chem. 410 (2018) 7679–7687, https://doi.org/10.1007/s00216-018-1383-1.

[41] L. Mahler, M. Tovar, T. Weber, S. Brandes, M.M. Rudolph, J. Ehgartner, T. Mayr, M.T. Figge, M. Roth, E. Zang, Enhanced and homogeneous oxygen availability during incubation of microfluidic droplets, RSC Adv. 5 (2015) 101871–101878, https://doi.org/10.1039/c5ra20118g.

[42] A. Ruszczak, P. Jankowski, S.K. Vasantham, O. Scheler, P. Garstecki, Physicochemical properties predict retention of antibiotics in water-in-oil droplets, Anal. Chem. 95 (2023) 1574–1581, https://doi.org/10.1021/acs.analchem.2c04644.

[43] T. Weber, S. Hengoju, A. Samimi, M. Roth, M. Tovar, M.A. Rosenbaum, Recovery and isolation of individual microfluidic picoliter droplets by triggered deposition, Sens. Actuators B Chem. 369 (2022) 132289, https://doi.org/10.1016/J.SNB.2022.132289.

Ashkan Samimi: 2012–2016 Bachelor of Engineering, Bonab University, Iran; 2016–2019 MSc in Photonics, Shahid Beheshti University, Iran. Since 2019 PhD studies in the microfluidics group at the Bio Pilot Plant of Leibniz HKI, Jena

Sundar Hengoju: 2007–2011 BTech in Biotechnology, Kathmandu University, Nepal; 2013–2015 Studies in Biochemistry (MSc) at Chungbuk National University, South Korea. 2016–2020 Ph.D. studies at Bio Pilot Plant of the Leibniz HKI and Friedrich Schiller University of Jena. Since 2020 Postdoc at Leibniz-HKI, Jena for droplet-based microfluidics.

Miriam A. Rosenbaum: 1999–2004 Diploma Studies in Biochemistry at the University of Greifswald, 2006 Ph.D. in Environmental Chemistry at the same place. 2007–2011 Postdoc Washington University and Cornell University, USA. 2011–2017 Assistant Professor in Applied Microbiology at the RWTH Aachen. Since 2017 Professorship for Synthetic Biotechnology at Friedrich Schiller University of Jena and Department Chair of the Bio Pilot Plant at Leibniz-HKI, Jena, Germany.